Quasifree pion scattering at 500 MeV

J. E. Wise, M. R. Braunstein, S. Høibråten, M. D. Kohler, B. J. Kriss, J. Ouyang, and R. J. Peterson
Nuclear Physics Laboratory, University of Colorado, Boulder, Colorado 80309

J. A. McGill, C. L. Morris, S. J. Seestrom, R. M. Whitton, and J. D. Zumbro
Los Alamos National Laboratory, Los Alamos, New Mexico 87545

C. M. Edwards
University of Minnesota, Minneapolis, Minnesota 55455

A. L. Williams
University of Texas, Austin, Texas 78712
(Received 12 May 1993)

Non-charge-exchange inclusive cross sections have been measured at 500 MeV incident pion energy at quasifree scattering kinematics for both positive and negative pion charges. Peaks identified with quasifree knockout are seen at momentum transfers from 314 to 724 MeV/c. The widths and sizes of the peaks seen are consistent with the knockout of single nucleons from the nuclear surface. The data are consistent with no softening of the pion quasifree response at high momentum transfer, in contrast to the result seen in 500-MeV pion charge exchange data.

PACS number(s): 25.80.Ls

I. INTRODUCTION

In quasifree scattering experiments, the incident particle transfers sufficient momentum to the target nucleus that the interaction can be considered to occur with a single constituent nucleon. A simple model of this process might assume the nucleus to be composed of a gas of noninteracting fermions and that the incoming projectile strikes a single one of these constituents, knocking it directly out of the nucleus. This Fermi gas model of quasifree scattering in the nonrelativistic impulse approximation predicts the quasifree process to occur at energy losses of $q^2/2M$, where q is the laboratory three-momentum transfer and M is the nucleon mass. Experimental measurements of the inclusive scattering cross section as a function of energy loss should thus show a peak at this energy loss, broadened as a result of the internal motion of the individual nucleons inside the nucleus. Studies of such inclusive electron scattering experiments in the quasifree regime [1], however, have shown this to be an inadequate description of the nuclear structure, implying that many-body corrections are needed even at high-momentum transfer and energy losses. These results are confirmed by exclusive $(e, e'p)$ measurements, where individual shell-model orbitals are seen to be depleted relative to predictions from an independent particle model without the inclusion of short-range correlations [2].

Scattering experiments using strongly interacting probes can explore quite different features of the quasifree reaction. For instance, quasifree single charge exchange (SCX) experiments of 500 MeV pions have been shown to probe the isovector response [3], while measurements of polarization transfer observables in $(\mathbf{p}, p')$ and $(\mathbf{p}, \mathbf{n})$ experiments at quasifree kinematics have isolated the spin longitudinal and spin transverse response as a function of the momentum transfer [4–7]. Details of the reaction mechanism, such as multinucleon absorption and scattering can be also be studied in such reactions. Quasifree SCX reactions of pions near the Δ_{33} resonance have, for example, indicated that one should consider delta propagation within the nucleus as an integral part of the pion quasifree reaction mechanism, at least for pion scattering near resonance [8, 9].

The present experiment is the first measurement of the quasifree pion inclusive non-charge-exchange (NCX) cross section above the Δ_{33} resonance. Doubly differential NCX cross sections have been measured for five angles up to 90°, corresponding to momentum transfers at quasifree kinematics of approximately 314–724 MeV/c. In this work we interpret the results in terms of a simple model of the quasifree scattering process. The high-energy loss regime above the quasifree response of the present data set has been analyzed within an intranuclear cascade model and is presented elsewhere [10].

II. EXPERIMENT AND DATA ANALYSIS

Data were accumulated on the P^3 channel of the Los Alamos Meson Physics Facility (LAMPF) [11–14]. Typically, beam fluxes of 10^7 s^{-1} (10^6 s^{-1}) were obtained for positively (negatively) charged pions through the channel for an incident pion beam momentum of 624 MeV/c. In addition to momentum and charge selection through the channel, positively charged pions were selected by use of

absorbers that allowed particles of different mass to be separated by energy loss. Beam intensity was monitored by an ionization chamber, as well as with a sampling grid scintillator (SGS) [15, 16]. The rates determined from these two counters were monitored for consistency during the experiment. Additionally, the relative pion/proton ratio was determined from a signal gated on pulse-height from the SGS and monitored as a check on beam stability and reproducibility.

The scattered pions were momentum analyzed in the large acceptance spectrometer (LAS)[17], a QQD magnetic spectrometer with a maximum central momentum of 685 MeV/c. The dipole is vertically bending, with a nominal bend angle of 30° giving a solid angle of the spectrometer of 25 msr and momentum acceptance of ±10%. The spectrometer is equipped with a series of four multiwire proportional chambers located both before and after the dipole for trajectory reconstruction. Two scintillator detectors and a threshold gas Čerenkov counter were used for the trigger and particle identification.

Targets having an areal density of about 1 g/cm^2 were chosen for nuclei over a wide range of nucleon number, and corrections were made to account for the energy loss to the scattered pion through the target. The experimental energy resolution was determined to be 7.0 ± 1.4 MeV for π^+p elastic scattering.

Data were normalized to the free πp differential cross section as determined by the phase-shift code SAID [18], which gives the free π^+p (π^-p) single differential cross section to be 2.26 (1.61) mb/sr at a laboratory scattering angle of 50°. Energy loss spectra accumulated for pion scattering from CH_2 (polyethylene) targets of 1.12 and 0.560 g/cm^2 areal density were subtracted for background contributions from carbon and line-shape fit to obtain the hydrogen elastic cross section at each angle. For an angular sweep under identical beam conditions, normalizations obtained by comparing these measured cross sections to the SAID values varied by less than 5% for the π^+p data and by about 7% for the scattering of negatively charged pions.

Single differential cross sections ($d\sigma/d\Omega$) were obtained by fitting Gaussian line shapes to all peaks. An estimate of the model dependence in the background was included by fitting curves with polynomial, exponential, and no backgrounds to the data. The maximum difference in cross section obtained from these fits was added in as an additional model uncertainty to the final cross sections.

III. RESULTS AND INTERPRETATIONS

A. Extracted cross sections

Non-charge-exchange data for both pion charges on a wide range of targets were obtained from 30° to 90° over the quasifree region. Shown in Fig. 1 are the doubly differential cross sections, $d^2\sigma/d\Omega\, d\omega$ for 500 MeV pions scattered from natural carbon targets (98.9% ^{12}C), plotted as a function of energy loss ω, for laboratory scattering angles of 30°, 40°, 50°, and 70°. The energy loss is defined here as the difference between the initial and final laboratory kinetic energies of the scattered pion, $T_{\rm in} - T_f$.

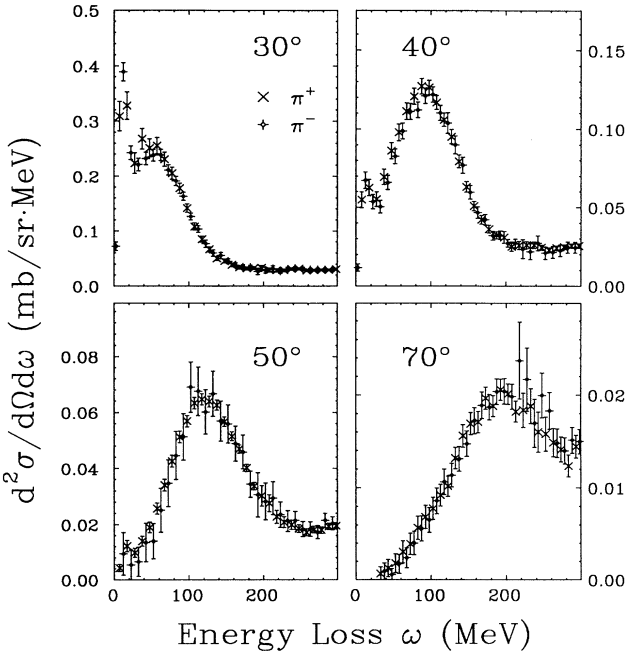

FIG. 1. Doubly differential cross sections $d^2\sigma/d\Omega d\omega$ plotted as a function of energy loss for 500 MeV charged pions scattered off of natural carbon from 30° to 70° lab scattering angle.

Both positive and negative pion cross sections are plotted in this figure. The cross sections are identical within statistics, as should be expected in the scattering of pions from a symmetric ($N = Z$) nucleus. The largest single feature in the data is a peak that appears at energy losses (ω) of approximately $q^2/2M$ in all scattering data, with a background that increases its size relative to the peak as one moves to a larger scattering angle. The peaks were fitted with a symmetric Gaussian lineshape to extract the full width at half maximum (FWHM) peakwidths, centroids, and areas. A symmetric Gaussian provided a reasonable description for the peakshape over the range of angles measured, though backgrounds at very low and at very high momentum transfers were large and made obtaining a reasonable fit difficult. For the 30° data, where contributions from Pauli blocking and the giant resonance region distort the quasifree peak shape, the cross section and widths have been extracted using a split Gaussian lineshape. Backgrounds were simultaneously fit to minimize the χ^2 and to obtain the single differential cross sections for each laboratory scattering angle.

Two major processes are thought to contribute to the background. Intranuclear cascade calculations [10] show pion production to be a substantial contribution to the inclusive cross section starting at about 150 MeV energy loss for 500 MeV pions at 50°. In addition, recent $(e, e'p)$ experiments [2, 19, 20] suggest an additional contribution from multinucleon knockout to the quasifree scattering cross section at high missing energy and momentum transfer. Since calculations of Mulders [21] show the two nucleon ($2N$) knockout contributions to the in-

clusive (e,e') cross section at momentum transfers of 400 MeV/c begin close to zero energy loss and peak in the dip region, we have modeled our background to simulate the combination of both pion production and multinucleon knockout starting at zero energy loss.

In Fig. 2 we show our data for the elastic and quasifree peaks at 500 MeV, 50° fit to symmetric Gaussian lineshapes, with both polynomial and exponential backgrounds. Calculated response functions for two nucleon knockout and delta production are shown as the dotted and dash-dotted curves, respectively. These response functions have been determined from a parameterization for (e,e') scattering in the quasifree region [22], and have been arbitrarily scaled to match the size of the background in the pion data. Electron scattering kinematics of 500 MeV, 66° (q=490 MeV/c for elastic scattering from a free proton) were chosen for this calculation approximately to reproduce the momentum transfer for quasifree scattering in the pion data. Exponential and polynomial fits provide similar estimates for the background of the pion data, and are seen to approximate the shape for the sum of the parameterized two-nucleon and pion production regions for (e,e'). The estimates for the uncertainties of the fitted single differential cross sections are dominated by the fit to the peaks with no background contribution. The model uncertainty of the background contribution for the 90° data has been taken as the difference between the fits with a polynomial and exponential background. These estimates are conservative for the low momentum transfer data, but may underestimate the contribution for the background at 90°.

The extracted cross sections from fits to the quasifree peak closely follow the free πN cross section. Shown in Fig. 3 are the extracted single differential cross sections $d\sigma/d\Omega$ plotted as a function of laboratory scattering angle obtained for natural carbon, calcium, zirconium, and ^{208}Pb. A phenomenological fit to the cross section using the parameterization

$$\frac{d\sigma}{d\Omega} = A_{\rm eff} B(q,k_F) \left(\frac{d\sigma}{d\Omega}\right)_{\pi N} \tag{1}$$

is shown as the solid lines in the figure. Here $B(q,k_F)$ is the Pauli blocking factor

$$B(q,k_F) = \begin{cases} \frac{3q}{4k_F} - \frac{q^3}{16k_F^3}, & \text{if } q < 2k_F; \\ 1, & \text{otherwise,} \end{cases} \tag{2}$$

where k_F is the Fermi momentum of the nucleons taken from the (e,e') data of Ref. [23] and $A_{\rm eff}$ is a parameter scaled to fit the data. For the free cross section the free $\pi^+ p$ (σ^+) and $\pi^- p$ (σ^-) scattering cross sections were used as obtained from the SAID calculated cross sections [18]. This elementary free cross section is averaged over all nucleons in the nucleus,

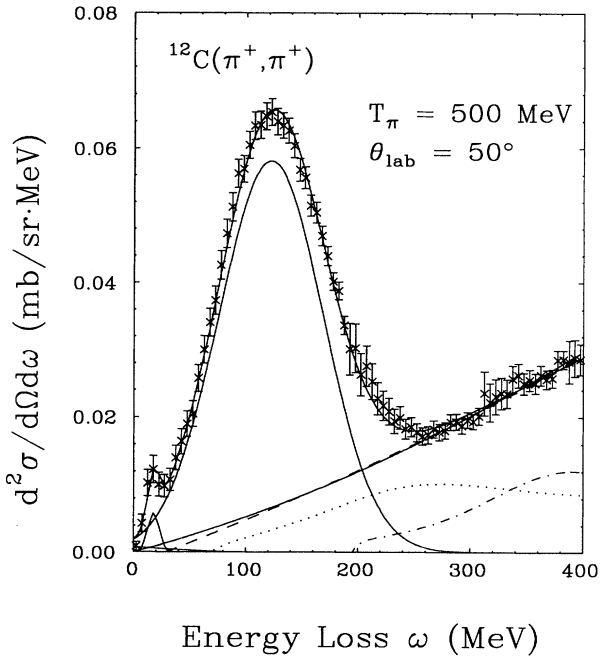

FIG. 2. Gaussian fit to 500 MeV, 50° ^{12}C(π^+,π^+) quasifree scattering data. A polynomial background fit to the data is given as a solid line, while the dashed line shows the best fit exponential background. The shape of the parameterized $2N$ response function for (e,e') from Ref. [22] is shown as the dotted line, while the dash-dotted line shows the shape of the delta production response function, also from Ref. [22].

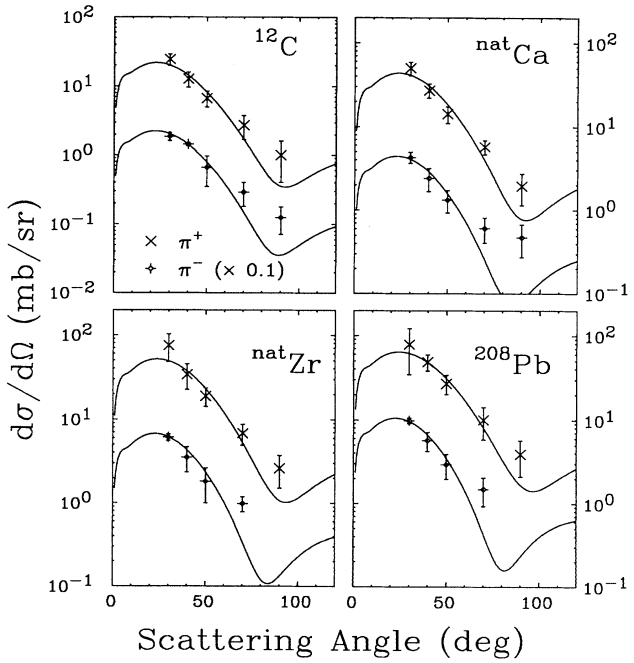

FIG. 3. Quasifree cross sections for the non-charge exchange 500 MeV π^+ and π^- data from natural carbon, calcium, zirconium, and ^{208}Pb targets as a function of laboratory scattering angle. A best fit to a Fermi gas model with an adjustable $A_{\rm eff}$ is shown as a solid line fits to the data. The negative pion data and fits have all been scaled by a factor of 0.1.

$$\left(\frac{d\sigma}{d\Omega}\right)_{\pi N} = \frac{Z\sigma^+ + (A-Z)\sigma^-}{A} \quad (3)$$

for the scattering of positively charged pions.

Cross sections were calculated at the momentum transfer of the incident pion, corrected for Coulomb effects:

$$q_{\text{eff}} = q\left[1 \pm \frac{4Z\alpha\hbar c}{3E_i r_0 A^{1/3}}\right] \quad (4)$$

where a radial parameter of $r_0 = 1.12$ fm has been used for the nuclear size. Here the plus sign corresponds to scattering of negatively charged pions from the target nucleus while a negative sign corresponds to positively charged pion scattering.

The Pauli-blocking term $B(q, k_F)$ in Eq. (1) produces a sharp falloff in the cross section at small momentum transfers. This is not noticeable in the data of Fig. 3 due to the lack of data at small angles. For these data only the scaling factor A_{eff} was fit to the data; the Fermi momentum k_F could not be determined from these fits and that parameter was therefore held constant at values determined from (e, e') experiments [23]. Values of 221, 251, 254, and 265 MeV/c were used for k_F in fits to the carbon, calcium, zirconium, and lead data, respectively. Best fit values for A_{eff} are given in Table I and are compared with the results of an eikonal calculation with a density distribution given by the charge density of the nucleus as determined from (e, e') measurements [26, 27].

Deviations of the data in Fig. 3 from the simple parameterization at large angles clearly indicate that nonquasifree processes are contributing to the cross section at these kinematics. The background dominates the fits at these large momentum transfers and clean extraction of the quasifree peak is difficult. Exclusive data at these momentum transfers may be useful in determining the different reaction channels contributing to the present inclusive results.

B. Nuclear shadowing

Data have been taken for a number of isotopes to obtain the A-dependence of the cross section; results for the effective number of nucleons A_{eff} as given by Eq. (3) are listed in Table I. The A-dependence follows a power law, as was seen for non-charge-exchange data taken near the Δ_{33} resonance [24, 25], and for 500 MeV charge exchange data taken on the LAMPF π^0 spectrometer [26]:

$$A_{\text{eff}} = N_0 A^{\alpha}. \quad (5)$$

Best fit values for the exponent α are found to be 0.44 ± 0.05 for the π^+ data, and 0.56 ± 0.03 for the π^- data. The result for α obtained in this analysis for positive pions is compatible with both the value of 0.43 ± 0.1 found in the 300 MeV non-charge-exchange data of Ref. [24] and the best fit value of 0.38 ± 0.03 from an analysis of the 500 MeV charge-exchange data [26], indicating a similar reaction mechanism is dominant in all three data sets. The larger value for the exponent for the scattering of negatively charged pions may indicate that processes other than quasifree knockout make a larger contribution in this reaction than in the others. For instance, absorption processes, which were found to scale with a larger value of the exponent in Ref. [24], might increasingly make a larger contribution to the cross section as we go to heavier nuclei for the negative pion data. Figure 4 shows a best fit of a power law (solid line) to the non-charge-exchange data for both pion charges, as well as the eikonal calculation of Ref. [26] (dotted line).

If the nucleus were transparent to the incoming charged pion, the cross section would be proportional to the number of nucleons in the target. A value less than one indicates shadowing of the free response by neighboring nucleons. Scattering from a totally absorbent black disk would scale as $A^{1/3}$. If the power law of Eq. (5) is assumed as a model, and the exponent α is then fit to the values for A_{eff} obtained from the eikonal calculation, a best fit is obtained for a value of $\alpha = 0.40$ (0.45) for positively (negatively) charged pions. These results are somewhat smaller than the fits to the data, but the enhancement of α for negatively charged pions seen from the analysis of the data is also seen in the calculation.

C. Extracted Fermi momenta

In a Fermi gas (FG) model, the width (FWHM) of the quasifree peak is related to the Fermi momentum and mass of the struck nucleon by the relationship

TABLE I. Calculated and measured values of A_{eff} for 500 MeV incident energy charged pions scattering from a number of nuclear targets. Columns 1 and 2 present the eikonal calculations of Ref. [26]. Experimental uncertainties are given in parentheses.

Target	Z	A	Eikonal π^+	Eikonal π^-	Experiment π^+	Experiment π^-
Li	3	7.0	3.53	3.69	3.3(0.9)	3.1(0.9)
C	6	12.0	4.45	4.45	3.8(0.5)	4.0(0.2)
Al	13	27.0	6.93	7.07	5.1(1.6)	5.1(2.1)
Ca	20	40.1	8.94	8.95	8.4(0.8)	8.4(1.0)
Zr	40	91.2	11.3	12.3	10.2(1.6)	12.8(1.1)
Sn	50	118.7	12.0	13.5	9.7(2.7)	9.7(4.8)
Ta	73	181.0	16.3	18.7		15.1(4.1)
Pb	82	208.0	14.0	16.5	14.0(2.0)	20.3(1.4)
U	92	238.1	15.5	18.3		17.9(4.9)

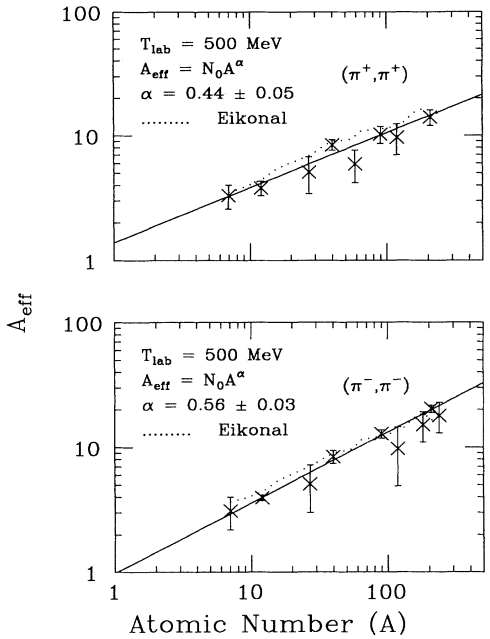

FIG. 4. Fit of the effective number of nucleons $A_{\rm eff}$ to a power law as a function of target nucleon number A. A best fit exponent of $\alpha = 0.44 \pm 0.05$ for positive pions is consistent with non-charge exchange data at 300 MeV [24] and charge-exchange results at 500 MeV. The dotted lines are the result of an eikonal calculation [26].

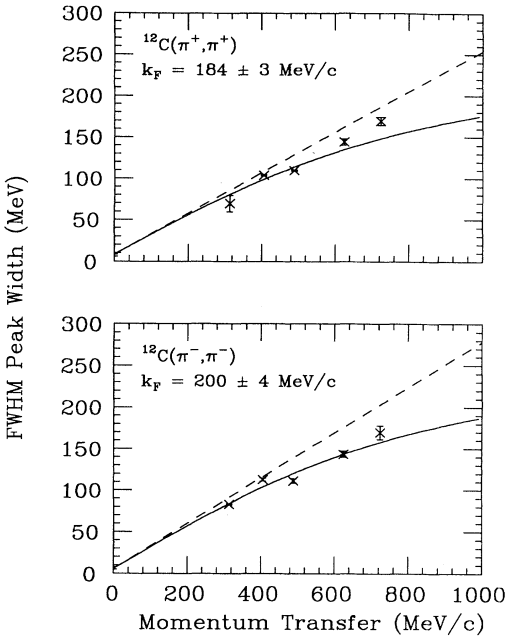

FIG. 5. FWHM widths from fits using a Gaussian lineshape to the quasifree peak of carbon, plotted as a function of momentum-transfer q. The best fit to the data is plotted as the solid (dashed) line in a Fermi gas model using relativistic (nonrelativistic) kinematics. Values of 184 ± 3 (200 ± 4) MeV/c are obtained in fits to the Fermi momentum k_F for the scattering of positively (negatively) charged pions from carbon, where relativistic kinematics and a nucleon mass given by its free value have been assumed.

$$\Gamma_{\rm FG} = \frac{1}{\sqrt{2}}\left(\sqrt{M^2 + (q + k_F)^2} - \sqrt{M^2 + (q - k_F)^2}\right), \tag{6}$$

where relativistic kinematics for the momentum transfer q have been used. In this equation, the quasifree cross section is taken to be that of the high-momentum transfer, unblocked limit of the free Fermi gas model and is thus parabolic in shape.

Shown in Fig. 5 are the widths of the peaks for the non-charge exchange data on carbon as a function of the laboratory three-momentum transfer q. The solid curve is a best fit to the peak widths using relativistic kinematics and the free mass of the nucleon, as given in Eq. (6), while the dashed curve is the result using nonrelativistic kinematics [3] for the same values of the fit parameters. The FWHM widths plotted here are for fits to a symmetric Gaussian (G) peak and polynomial background, with the uncertainties corresponding to changes in the fitted parameters so as to increase χ^2 by 1. Contributions from the uncertainty in the model for the background are large (about 15%) and are not included in these plotted data, but are included in the estimates for the uncertainties in the systematic errors for the fits of the parameters described below. For the 30° data, the width has been extracted using a split Gaussian lineshape.

For equal area curves, the FWHM of a fitted Gaussian is approximately related to the FWHM of the parabolic shape of the free Fermi gas model by $\Gamma_{\rm FG} = 1.13 \times \Gamma_{\rm G}$. A Gaussian was selected as a fitting function to allow the reliable extraction of both a width and a background, which was modeled as either a polynomial or exponential. For the 40° data, where backgrounds were small in the quasifree region, we fit the quasifree peak to both a symmetric Gaussian and a second-order polynomial. The results for $\Gamma_{\rm FG}$ from these two fits agreed to within 5%.

If M is taken as the free mass of the proton, $M = M_{\rm free}$, then the widths extracted from the fit to the data in this model give a Fermi momentum for carbon of 184 ± 3 MeV/c for positive pions and 200 ± 4 MeV/c for negatively charged pions. The choice of model for the shape of the peak and background is estimated to give an additional 10% uncertainty to these values. Our results are less than the value of 221 MeV/c as determined from electron scattering experiments and considerably less than the value for nuclear matter, 270 MeV/c. In the nonrelativistic Fermi gas model, however, we are only able to determine the ratio k_F/M. Thus, if we consider k_F fixed at the value determined from electron scattering, we find an effective nucleon mass of $1.20 \pm 0.01 \pm 0.18$ $M_{\rm free}$ ($1.11 \pm 0.02 \pm 0.20$ $M_{\rm free}$) from an analysis of the positive (negative) pion scattering data, where the uncertainties are given as the statistical and model contributions, respectively. Small enhancements of this order are predicted at the nuclear surface by extensions to mean-field theory [28, 29]. One explanation for the seemingly

low value of k_F (or large effective mass) is that the pions are being absorbed before reaching the nuclear interior, and thus are quasielastically scattered from only surface nucleons, that have, on the average, a much lower density. Similar effects were seen in the quasifree SCX data of Ref. [3]. The large model dependence resulting from the uncertainty of the peak shape and background, however, makes our results for ^{12}C compatible with the (e, e') data.

Fits to the widths have also been performed for several heavier nuclei. Fermi momenta of 221 ± 6, 200 ± 19, and 208 ± 21 MeV/c were obtained in fits to the positively charged pion data scattered from calcium, zirconium, and lead, respectively, where the free mass of the nucleon has been assumed and the uncertainty on the data points includes the model uncertainty discussed above for the fitting procedure. These values are much lower than that found from the inclusive (e, e') data, and are thus also consistent with the interpretation that the pions scatter from nucleons in the lower density, exterior regions of the nucleus.

D. Softening of the response

Separated transverse electron-scattering data in the quasifree regime show a consistent increase of the position of the quasifree peak relative to scattering from free kinematics as a function of momentum transfer. This is called a hardening of the response by several authors [30, 31] and is thought to be related to the inclusion of a repulsive interaction to the long range correlations in the calculation of the transverse response at high-momentum transfer. The residual particle-hole force used in these 1p1h random-phase approximation (RPA) calculations is found to be highly momentum-transfer dependent in the spin-longitudinal channel, becoming attractive at momentum transfers of about 1 fm^{-1}. In the spin-transverse channel, however, the force remains repulsive up until about 3 fm^{-1}. Thus spin-isospin sensitive probes may reflect this q-dependence of the residual interaction in the quasifree response. Transverse electron scattering samples mainly the volume spin-transverse response, and thus will feel the results of the repulsive particle-hole force at large momentum-transfer in that channel. Strongly interacting probes that contain mixtures of spin-longitudinal and spin-transverse channels may show a quite different momentum-transfer response [32, 33], but the effects due to the momentum-transfer dependence from the residual interaction may be difficult to disentangle from distortions entering the scattering process [31, 34].

In Fig. 6 we present the energy shift of the quasifree peak from free kinematics as a function of momentum transfer for the scattering of 500 MeV charged pions from carbon. Here the energy shift is defined as the difference in energy found between the fitted maxima of the carbon quasifree peak and the hydrogen elastic peak, taken from our CH_2 normalization runs at each angle. Uncertainties in the peak position due to the model for the peak lineshape and backgrounds have been estimated and are included in the data of Fig. 6. Our data are consistent

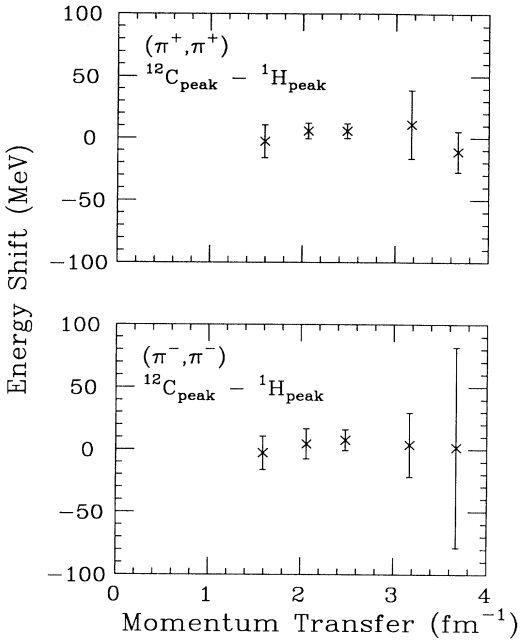

FIG. 6. Energy shifts of the ^{12}C quasifree peak relative to scattering from hydrogen. An increasing value of the shift at large momentum transfer would indicate a "hardening" of the response, while a decreasing value would indicate a "softening" of the quasifree response.

with a constant dependence on momentum transfer; no significant softening of the response is seen for values of the momentum transfer up to about 3 fm^{-1}, though the large uncertainty in the observed peak position above this value does not preclude this possibility at very high-momentum transfers. This result contrasts with the softening above 2 fm^{-1} seen in the 500 MeV pion SCX data of Ref. [3]. Such SCX reactions probe the isovector response of the nucleus to the external probe, while the present NCX reaction is largely isoscalar [18, 35]. Indeed, recent calculations performed within the framework of Fermi liquid theory show that the quasifree peak position should be located at exactly the free value for the scattering of isoscalar probes [36], while the energy shift for isovector probes will be positive. This is consistent with the present results. It is therefore tempting to ascribe the difference between the quasifree peak position in the SCX and NCX data as due to the momentum-transfer dependence of different channels of the residual interaction. However, there are several competing factors that could cause shifts in the peak positions, such as distortions in the scattering process [3, 31, 34] or a shift in the shape of the inclusive cross section as a result of a momentum-transfer dependent occupancy of the individual orbitals involved in the scattering process [9, 37]. If one assumes charge symmetry, then all distortions for SCX and NCX reactions from $T = 0$ nuclei are the same, and thus would not explain the observed shifts for carbon. However, there has been some evidence in recent electron-scattering measurements [2, 19, 20] for a momentum-transfer dependence in the relative spectro-

scopic amplitudes for protons in the p shell of ^{12}C, as well as for the Landau parameter [38, 39] g'. Such effects might not be expected to be a large contribution for the quasifree scattering of pions at 500 MeV, but cannot presently be excluded as possible explanations for any observed energy shifts of the quasifree peak position with respect to calculated values.

E. Interprobe comparison

In the impulse approximation the quasifree cross section is proportional to the free probe constituent cross section, a kinematic factor to account for the phase space factors in the reaction, and to a response function dependent only upon the internal structure of the target nucleus. We have seen in the previous sections that for 500 MeV pions, the single differential quasifree cross section scales with the free πN cross section over a wide range of kinematics, implying that the major consequence of the distortions and kinematic factor in the scattering process is an attenuation of the impulse approximation result. Thus, by dividing out the free πN cross section from our doubly differential cross section, we should obtain approximately the nuclear response for that scattering process attenuated by some overall scale factor.

In Fig. 7 we present the ^{12}C response function for NCX scattering at 500 MeV, 50°, which corresponds to a momentum transfer for scattering from a free proton of 488 MeV/c. Also shown in Fig. 7 are the SCX data of Ref. [26] at the same momentum transfer. These response functions are defined as the doubly differential cross section divided by the product of the elementary probe-constituent single differential cross section and the fitted scale factor $N_{\rm eff}$:

$$R(q,\omega) = \frac{d^2\sigma}{d\Omega d\omega}\left[N_{\rm eff}\left(\frac{d\sigma}{d\Omega}\right)_{\pi N}\right]^{-1} \tag{7}$$

In this equation the elementary πN cross section is given by Eq. (3) for the NCX reaction, and $N_{\rm eff}$ is the effective number of nucleons that participate in the reaction, given by the fitted scale parameter $A_{\rm eff}$ for the NCX data. When plotted in this manner, the response functions are nearly identical, indicating that we are probing similar aspects of the internal nuclear structure with these two reactions. It should be remembered, however, that these are not constant q surfaces; the momentum transfer varies by about 5% over the width of the quasifree peak at these kinematics, and thus the comparison is not precise. In addition, background not associated with single nucleon knockout is included in these plots, so some caution should be exercised in too literal a comparison between these two figures.

Nonetheless, presenting the data in this format may be useful. For comparison, the separated longitudinal charge response function $[R_L(q,w)/C(q)]$ for quasifree (e,e') at approximately the same momentum transfer [40] is shown at the bottom of Fig. 7, where the normalization factor $C(q)$ is the measured Coulomb sum rule,

$$C(q) = \int R_L(q,\omega)d\omega \tag{8}$$

determined from the same experiment. It should be noted that here $C(q)$ includes kinematic recoil factors, nucleon form factors, as well as some nuclear structure effects, so one should not expect it to equal the high-momentum-transfer limit for the no-correlation result of $C(q) = Z = 6$ for ^{12}C.

In Fig. 8, we present the NCX, SCX, and (e,e') response functions as defined above at a momentum transfer of approximately 300 MeV/c. The Second RPA (SRPA) calculation of Ref. [41] is presented with the (e,e') data, separated into the $T = 0$ and $T = 1$ channels. The effective interaction used in these calculations has been constructed from a G matrix in nuclear matter derived from a one-boson exchange potential [42]. The calculated longitudinal charge response contains an approximately equal mixture of isoscalar and isovector components. The predicted shapes for the isospin components of the charge response are plotted as solid curves in (a) and (b) with the pion data. From this comparison we would correctly expect the NCX data to be predominantly isoscalar, while the SCX response would be isovector. In addition, we note that even when $2p2h$ correlations are specifically included in a calculation of the response, as it is in the SRPA results, the centroid energy of the isoscalar response is softened with respect to the isovector response at low-momentum transfer in accordance with our results from the previous section.

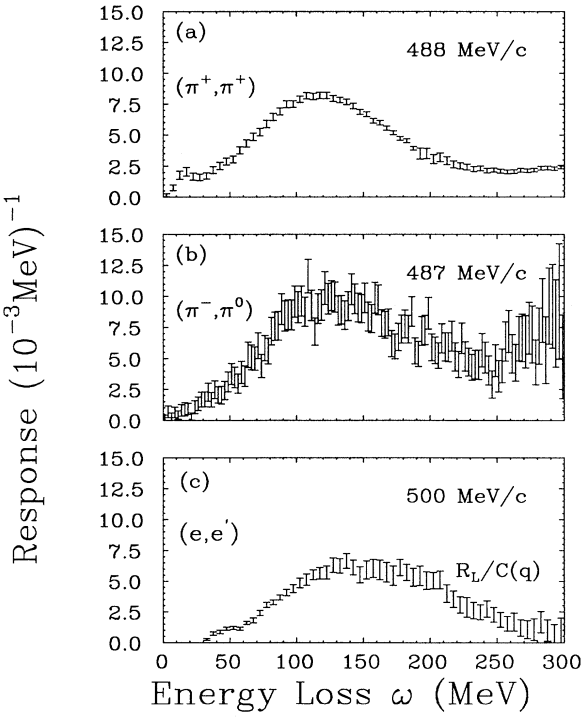

FIG. 7. Response functions for ^{12}C at a momentum transfer of approximately 500 MeV/c for (a) pion NCX, (b) pion SCX, and (c) (e,e').

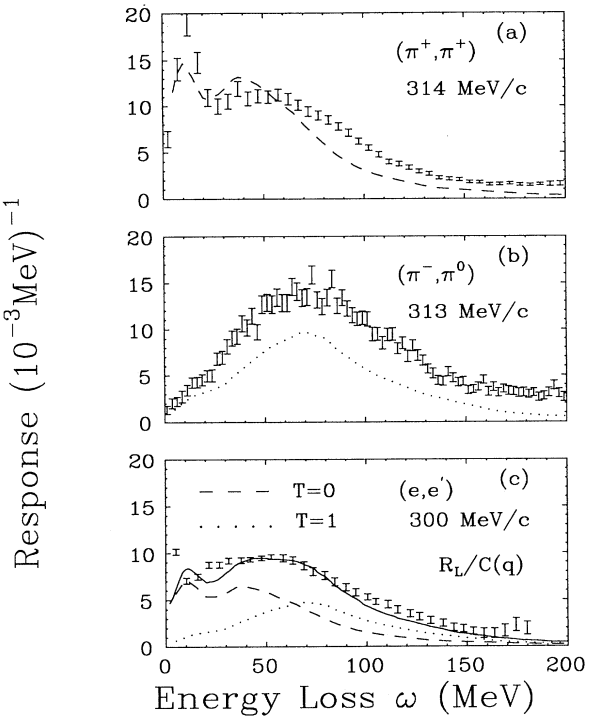

FIG. 8. Response functions for ^{12}C at a momentum transfer of approximately 300 MeV/c for (a) pion NCX, (b) pion SCX, and (c) (e,e'). Curves in (c) from Ref. [41] show the longitudinal charge response separated into isoscalar (dashed line) and isovector (dotted line) components. Curves drawn in (a) and (b) are the isoscalar and isovector components, respectively, from (c), multiplied by a factor of 2.0.

IV. CONCLUSIONS

Inclusive data have been accumulated for charged pion scattering at 500 MeV for scattering angles from 30° to 90°. Doubly differential cross sections show a maximum at kinematics corresponding to quasifree single nucleon knockout. Single differential cross sections extracted from these data scale with the free πN cross section and are thus consistent with scattering from a Fermi gas of noninteracting nucleons. Values of the effective number of nucleons seen in the scattering are, however, consistent with a quasifree scattering process from only about a third of the nucleons inside the nucleus. This is similar to the results found in recent SCX pion quasifree data taken at similar kinematics. Though the width of the quasifree peak is proportional to the momentum transfer, as would be expected in a simple Fermi gas picture, the width extracted from the simple Fermi gas model is consistent with a low value of the Fermi momentum. One explanation of this could be that the pions are absorbed in the low density region of the nuclear exterior, and thus quasifree knockout would reflect the structure of the nucleus only in this exterior region.

The lack of a significant "softening" of the response is in contrast to what was found with comparable 500 MeV SCX reactions. Because the SCX reaction is isovector while the present NCX is largely isoscalar, we may be seeing a momentum-transfer dependence from different channels of the residual interaction. However, there are several competing mechanisms that could shift the maximum of the observed quasifree peak, so this explanation must remain tentative.

Though the results from the widths and A-dependence of the quasifree peaks from the present analysis indicate that the pion is largely absorbed at the nuclear surface, calculations at large energy losses [10] indicate that the nucleus is relatively transparent to pions at these energies. In addition, these calculations show that a major component of the background is pion production at large energy losses. Future kinematically complete $(\pi,\pi p)$ and $(\pi,2\pi)$ reactions above resonance would be helpful in identifying both the reaction mechanism and structure of the target nucleus seen at these large momentum transfers and energy losses.

Finally, the presentation of NCX, SCX, and the (e,e') inclusive data in terms of a phenomenological response function suggests that the underlying reaction mechanism for these data are the same—the quasifree scattering from constituent nucleons inside the target nucleus. Distortions from the nuclear medium are seen to mainly attenuate the cross section relative to impulse approximation predictions. Other processes clearly enter, since the backgrounds grow increasingly large as the momentum transfer is increased, dominating the cross section at the largest angles we measure. The identification of the kinematic regime over which these different processes occur is an important area for future exclusive experiments, though these may be initially explored in inclusive measurements by the observation of scaling behavior at large momentum transfers and energy losses [43]. Such techniques, already successfully applied to the analysis of quasifree data using the weakly interacting electromagnetic interaction, might be useful in the analysis of mesonic quasifree data, as well as for other reactions where distortions in the scattering process are relatively small.

ACKNOWLEDGMENTS

The authors would like to thank the LAMPF staff for assistance in the setup and running of this experiment, and to J. M. Finn and M. Holcomb for their help in providing electron-scattering data. This work has been funded in part under Contract No. DE-FG02-86ER-40296 from the Department of Energy.

[1] R. Altemus, A. Cafolla, D. Day, J. S. McCarthy, R. R. Whitney, and J. E. Wise, Phys. Rev. Lett. **44**, 965 (1980).

[2] L. B. Weinstein, H. Baghaei, W. Bertozzi, J. M. Finn, J. Glickman, C. E. Hyde-Wright, N. Kalantar-Nayestanaki, R. W. Lourie, J. A. Nelson, W. W. Sapp, C. P. Sargent, P. E. Ulmer, B. H. Cottman, L. Ghedira, E. J. Winhold, J. R. Calarco, J. Wise, P. Boberg, C. C. Chang, D. Zhang, K. Aniol, M. B. Epstein, D. J. Margaziotis, C. Perdrisat, and V. Punjabi, Phys. Rev. Lett. **64**, 1646 (1990).

[3] R. J. Peterson, S. Høibråten, J. Ouyang, M. R. Braunstein, X. Y. Chen, M. D. Kohler, B. J. Kriss, D. J. Mercer, D. S. Oakley, and D. L. Prout, Phys. Lett. B **297**, 238 (1992).

[4] *Spin Excitations in Nuclei*, edited by F. Petrovich, G. E. Brown, G. T. Garvey, C. D. Goodman, R. A. Lindgren, and W. G. Love (Plenum, New York, 1982).

[5] T. A. Carey, K. W. Jones, J. B. McClelland, J. M. Moss, L. B. Rees, N. Tanaka, and A. D. Bacher, Phys. Rev. Lett. **53**, 144 (1984).

[6] X. Y. Chen, L. W. Swenson, F. Farzanpay, D. K. McDaniels, Z. Tang, Z. Xu, D. M. Drake, I. Bergqvist, A. Brockstedt, F. E. Bertrand, D. J. Horen, J. Lisantti, K. Hicks, M. Vetterli, and M. J. Iqbal, Phys. Lett. B **205**, 436 (1988); Nucl. Phys. **A505**, 670 (1989).

[7] J. B. McClelland, T. N. Taddeucci, X. Y. Chen, W. P. Alford, R. C. Byrd, T. A. Carey, S. DeLucia, C. D. Goodman, E. Gülmez, W. Huang, B. Luther, D. G. Marchlenski, D. J. Mercer, D. L. Prout, J. Rapaport, L. J. Rybarcyk, W. Sailor, E. Sugarbaker, Y. Wang, and C. Whitten, Jr., Phys. Rev. Lett. **69**, 582 (1992).

[8] S. Høibråten, S. Gilad, W. J. Burger, R. P. Redwine, E. P. Piasetzky, H. W. Baer, J. D. Bowman, F. H. Cverna, F. Irom, M. J. Leitch, J. N. Knudson, S. A. Wood, and S. H. Rokni, Phys. Rev. C **43**, 1255 (1991).

[9] M. Thies, Nucl. Phys. **A382**, 434 (1982).

[10] J. D. Zumbro, J. E. Wise, M. R. Braunstein, M. D. Kohler, B. J. Kriss, S. Høibråten, J. A. McGill, C. L. Morris, R. J. Peterson, J. Ouyang, C. M. Edwards, S. J. Seestrom, R. M. Whitton, and A. L. Williams, Phys. Rev. Lett. **71**, 1796 (1993).

[11] M. S. Livingston, LAMPF internal Report No. LA-6878-MS, 1977.

[12] *The* P^3 *Reference Manual*, compiled by R. E. Morgado, LAMPF, Los Alamos, New Mexico, 1982 (unpublished).

[13] R. D. Werbeck and R. J. Macek, IEEE Trans. Nucl. Sci. **NS-22**, 1598 (1975).

[14] W. J. Briscoe, D. H. Fitzgerald, B. M. K. Nefkens, and M. E. Sadler, Nucl. Instrum. Methods **197**, 277 (1982).

[15] J. Ouyang, private communication.

[16] W. R. Holley, G. L. Schnurmacher, and A. R. Zingher, Nucl. Instrum. Methods **171**, 11 (1980).

[17] E. Colton, Nucl. Instrum. Methods **178**, 95 (1980).

[18] R. A. Arndt and L. D. Roper, program SAID, Virginia Polytechnic Institute and State University, Blacksburg, Virginia, 1990, solution SM90; R. A. Arndt, Z. Li, L. D. Roper, R. L. Workman, and J. M. Ford, Phys. Rev. D **43**, 2131 (1991).

[19] J. Morrison, Ph.D. dissertation, MIT, 1993 (unpublished).

[20] R. W. Lourie, W. Bertozzi, J. Morrison, and L. B. Weinstein, Phys. Rev. C **47**, 444 (1993).

[21] P. J. Mulders, Nucl. Phys. **A459**, 525 (1986).

[22] J. W. Lightbody, Jr. and J. S. O'Connell, Comput. Phys. (May/June 1988), p. 57.

[23] R. R. Whitney, I. Sick, J. R. Ficenec, R. D. Kephart, and W. P. Trower, Phys. Rev. C **9**, 2230 (1974).

[24] D. Ashery, I. Navon, G. Azuelos, H. K. Walter, H. J. Pfeiffer, and F. W. Schlepütz, Phys. Rev. C **23**, 2173 (1981).

[25] S. M. Levenson, D. F. Geesaman, E. P. Colton, R. J. Holt, H. E. Jackson, J. P. Schiffer, J. R. Specht, K. E. Stephenson, B. Zeidman, R. E. Segel, P. A. M. Gram, and C. A. Goulding, Phys. Rev. C **28**, 326 (1983).

[26] J. Ouyang, Ph.D. dissertation, University of Colorado, 1992.

[27] H. De Vries, C. W. De Jager, and C. De Vries, At. Nucl. Data Tables **36**, 495 (1987).

[28] Z. Y. Ma and J. Wambach, Nucl. Phys. **A402**, 275 (1983).

[29] G. F. Bertsch and T. T. S. Kuo, Nucl. Phys. **A112**, 204 (1968).

[30] W. M. Alberico, M. Ericson, and A. Molinari, Nucl. Phys. **A379**, 429 (1982).

[31] A. De Pace and M. Viviani, Phys. Lett. B **236**, 397 (1990).

[32] W. M. Alberico, A. De Pace, M. Ericson, Mikkel B. Johnson, and A. Molinari, Phys. Rev. C **38**, 109 (1988).

[33] I. Bergqvist, A. Brockstedt, L. Carlén, L. P. Ekström, B. Jakobsson, C. Ellegaard, C. Gaarde, J. S. Larsen, C. Goodman, M. Bedjidian, D. Contardo, J. Y. Grossiord, A. Guichard, R. Haroutunian, J. R. Pizzi, D. Bachelier, J. L. Boyard, T. Hennino, J. C. Jourdain, M. Roy-Stephan, M. Boivin, and P. Radvanyi, Nucl. Phys. **A469**, 648 (1987).

[34] M. Ichimura, K. Kawahigashi, T. S. Jørgensen, and C. Gaarde, Phys. Rev. C **39**, 1446 (1989).

[35] J. M. Eisenberg and D. S. Koltun, *Theory of Meson Interactions with Nuclei* (Wiley, New York, 1980), p. 11.

[36] J. Wambach, Phys. Rev. C **46**, 807 (1992).

[37] K. Wehrberger and F. Beck, Phys. Lett. B **266**, 1 (1991).

[38] J. E. Wise, J. R. Calarco, J. P. Connelly, S. A. Fayans, F. W. Hersman, J. H. Heisenberg, R. S. Hicks, W. Kim, T. E. Milliman, R. A. Miskimen, G. A. Peterson, A. P. Platonov, E. E. Saperstein, and R. P. Singhal, Phys. Rev. C **47**, 2539 (1993).

[39] W. Kim, A. P. Platonov, and E. E. Saperstein, Yad. Fiz. **56**, 109 (1993) [Phys. At. Nucl. **56**, 1213 (1993)].

[40] P. Barreau, M. Bernheim, J. Duclos, J. M. Finn, Z. Meziani, J. Morgenstern, J. Mougey, D. Royer, B. Saghai, D. Tarnowski, S. Turck-Chieze, M. Brussel, G. P. Capitani, E. De Sanctis, S. Frullani, F. Garibaldi, D. B. Isabelle, E. Jans, I. Sick, and P. D. Zimmerman, Nucl. Phys. **A402**, 515 (1983).

[41] S. Drożdż, S. Nishizaki, J. Speth, and J. Wambach, Phys. Rep. **197**, 1 (1990).

[42] K. Nakayama, S. Krewald, J. Speth, and W. G. Love, Nucl. Phys. **A431**, 419 (1984).

[43] D. B. Day, J. S. McCarthy, T. W. Donnelly, and I. Sick, Annu. Rev. Nucl. Part. Sci. **40**, 357 (1990).